MESOSCOPIC PHYSICS

Counter-propagating charge transport in the quantum Hall effect regime

Fabien Lafont[1,2]*†, Amir Rosenblatt[1]*, Moty Heiblum[1], Vladimir Umansky[1]

The quantum Hall effect, observed in a two-dimensional (2D) electron gas subjected to a perpendicular magnetic field, imposes a 1D-like chiral, downstream, transport of charge carriers along the sample edges. Although this picture remains valid for electrons and Laughlin's fractional quasiparticles, it no longer holds for quasiparticles in the so-called hole-conjugate states. These states are expected, when disorder and interactions are weak, to harbor upstream charge modes. However, so far, charge currents were observed to flow exclusively downstream in the quantum Hall regime. Studying the canonical spin-polarized and spin-unpolarized $\nu = 2/3$ hole-like states in GaAs-AlGaAs heterostructures, we observed a significant upstream charge current at short propagation distances in the spin unpolarized state.

Elementary charge excitations in the quantum Hall effect (QHE) flow downstream along the edge of a two-dimensional electron gas (2DEG), with the downstream chirality imposed by the magnetic field (*1*). In the fractional regime (*2*), this statement remains valid only for particle-like (Laughlin's) states (*3*–*5*); by contrast, hole-like states (filling factors υ so that $1/2 + n < \upsilon < 1 + n$ with $n = 0, 1, 2...$) are expected to harbor counter-propagating (downstream and upstream) charge excitations (*6*). In a noninteracting and scattering-free model, a downstream $\upsilon = 1$ charge mode was predicted to be accompanied by an upstream $\upsilon = 1/3$ mode, leading to a two-terminal conductance of $4e^2/3h$, where e and h are the electron charge and the Planck constant, respectively. However, experimentally, only downstream charge modes (*7*, *8*) with a two-terminal conductance of $2e^2/3h$ accompanied by upstream neutral modes (*9*–*15*) have been found. A recent experiment (*16*) measured conductance of an unequilibrated downstream channels at narrow regions (4 μm wide) of the polarized $\upsilon = 2/3$ state; the results were consistent with the model from (*6*), but no direct measurement of the upstream current was made. Although the majority of the studies were concentrated on the spin-polarized $\upsilon = 2/3$ state, there has been recent interest in its spin-unpolarized counterpart (*17*–*24*) as a potential host for para-fermions when coupled to superconducting contacts (*25*–*27*). In the composite fermion (CF) picture, one can construct two kinds of states in the $\upsilon = 2/3$: an unpolarized state, emerging at lower magnetic fields, with two quantum levels that have the same orbital quantum number but opposite spin configurations: (0, ↑) and (0, ↓) (Fig. 1B) (*28*), and a polarized state, emerging at high magnetic fields, with two quantum levels having the same spin but different orbitals (0, ↑) and (1, ↑) (*29*). The majority of previous experiments in the unpolarized state focused on characterizing the spin domains structure in the bulk (*23*, *24*, *30*) or the nuclear spin polarization occurring at high currents (*18*, *19*, *21*, *22*, *30*–*35*). Still, the configuration of edge channels for this state remains elusive: On the one hand, no upstream channel is expected in the CF picture; on the other, because the effective K-Matrix in the CF basis is the same for both $\upsilon = 2/3$ states, an upstream mode should occur also in the unpolarized case (*36*). We studied the two flavors of the $\upsilon = 2/3$ state along a short distance (a few micrometers) and found a substantial upstream charge current only in the spin-unpolarized state. Consequently, the two-terminal resistance deviates from the quantized one at $\upsilon = 2/3$. The GaAs-AlGaAs heterostructure used to study the two $\upsilon = 2/3$ states had to be carefully designed (with the 2DEG confined in a narrow, 12-nm-wide quantum-well) because we aimed to have the transition between the two states at a sufficiently high carrier density (and magnetic field), corresponding to having high mobility throughout the transition region in the phase space between the two states. A conductive n^+ GaAs layer was grown ~1 μm below the 2DEG and served as a backgate, capable of tuning the density from 1×10^{11} to 2.5×10^{11} cm^{-2}, with a corresponding low-temperature dark mobility of 1.5×10^6 to 3.5×10^6 cm^2 V^{-1} s^{-1}. Lock-in measurements were performed at ~80 Hz with an input current $I = 1$ nA and an electron temperature of ~35 mK [additional fabrication information is provided in (*37*), section 1].

The evolution of the four-terminal longitudinal (R_{xx}) and transverse resistance (R_{xy}), measured in a 40-μm-wide Hall-bar geometry, is plotted on Fig. 1, A and C. As reported previously (*17*, *21*, *22*, *30*, *31*), a clear transition between the two-spin varieties of the $\upsilon = 2/3$ states is visible in R_{xx} (around $V_{bg} = -0.5$ V and $B = 10$ T) (Fig. 1A). The finite R_{xx} region corresponds to the point at which the system undergoes a first-order quantum phase transition between the spin-unpolarized and the spin-polarized $\upsilon = 2/3$ state. The transverse resistance $R_{xy} \simeq (2e^2/3h)^{-1} \simeq$ 38.7 kilohms, however, remains constant on both sides of the transition. As predicted in (*6*), the presence of an upstream current leads to the

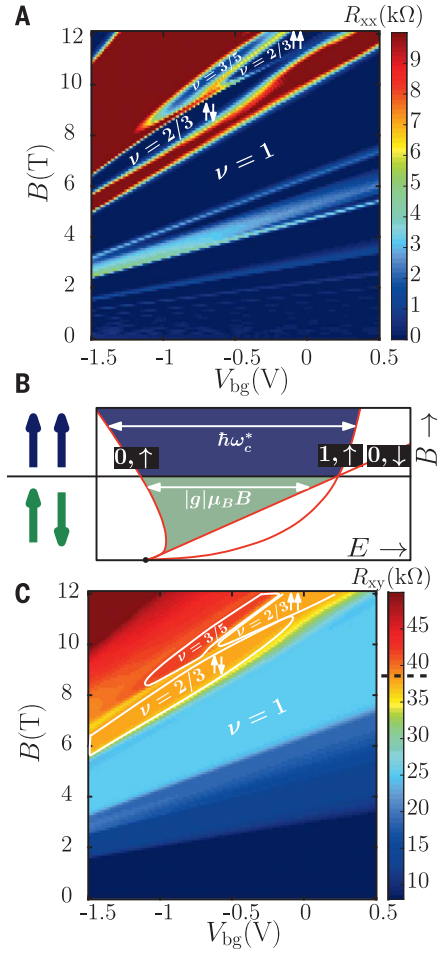

Fig. 1. Longitudinal and transverse magnetoresistances measured in a 40-μm-wide Hall bar sample. (**A**) Longitudinal four-terminal magnetoresistance versus backgate voltage measured by using $I = 1$ nA at $T = 40$ mK. A clear nondissipated state, $R_{xx} \approx 0$, is visible for the $\nu = 2/3$ polarized and unpolarized states. (**B**) Sketch of the evolution of the relevant energy scales. At low field, a gap exists between the (0, ↑) and (0, ↓) states,corresponding to the spin unpolarized state, whereas at higher fields, thanks to the different B dependency of the Coulomb ($\propto l_B^{-1} \sim \sqrt{B}$, where l_B is the magnetic length) and Zeeman ($\propto B$) energies, the gap exists between the (0, ↑) and the (1, ↑) λ levels corresponding to the polarized state. (**C**) Four-terminal transverse magnetoresistance as function of the backgate voltage. The $\nu = 2/3$ polarized and unpolarized quantum Hall plateaus exhibit a resistance $R_{xy} \approx (2e^2/3h)^{-1} \approx$ 38.7 kilohms (dashed line on the color bar).

[1]Braun Center for Submicron Research, Department of Condensed Matter Physics, Weizmann Institute of Science, Rehovot 76100, Israel. [2]College de France, 11 place Marcelin Berthelot, 75231 Paris Cedex 05, France.
*These authors contributed equally to this work.
†Corresponding author. Email: lafont.fabien@gmail.com

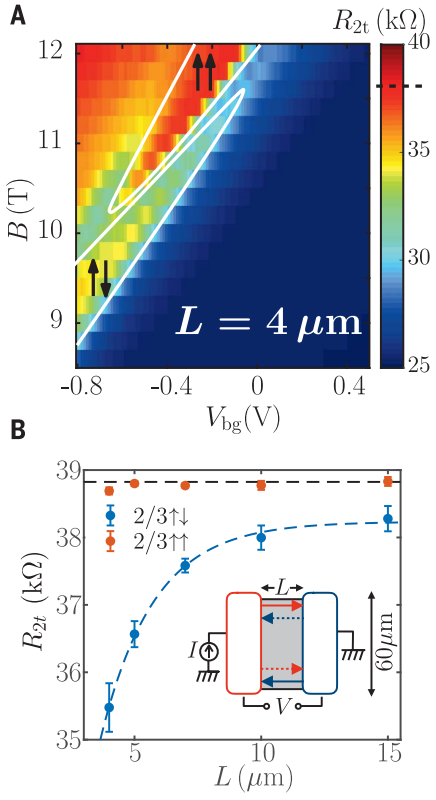

Fig. 2. Deviation from the quantized Hall resistance value owing to the upstream current. (**A**) Two-terminal magnetoresistance versus backgate voltage for a L = 4-μm-long and 60-μm-wide sample measured at T ~ 35 mK and I = 1 nA. A clear difference appears between the spin-polarized state, which remains quantized, and the spin-unpolarized state, which deviates substantially from the quantized value. (**B**) Evolution of the two-terminal resistance averaged over an area of (B, V_{bg}) corresponding to the polarized and unpolarized $\nu = 2/3$ states, as a function of the length L [(*38*), section 2]. The dashed black line is the quantized value $(2e^2/3h)^{-1}$, and the dashed blue line is an exponential fit $R(x) = [R(0) - R(\infty)]e^{-x/l_0} + R(\infty)$, where $R(0)$ = 20 ± 13 kilohms, $R(\infty)$ = 38.2 ± 0.3 kilohms, and l_0 = 2.1 ± 0.8 μm.

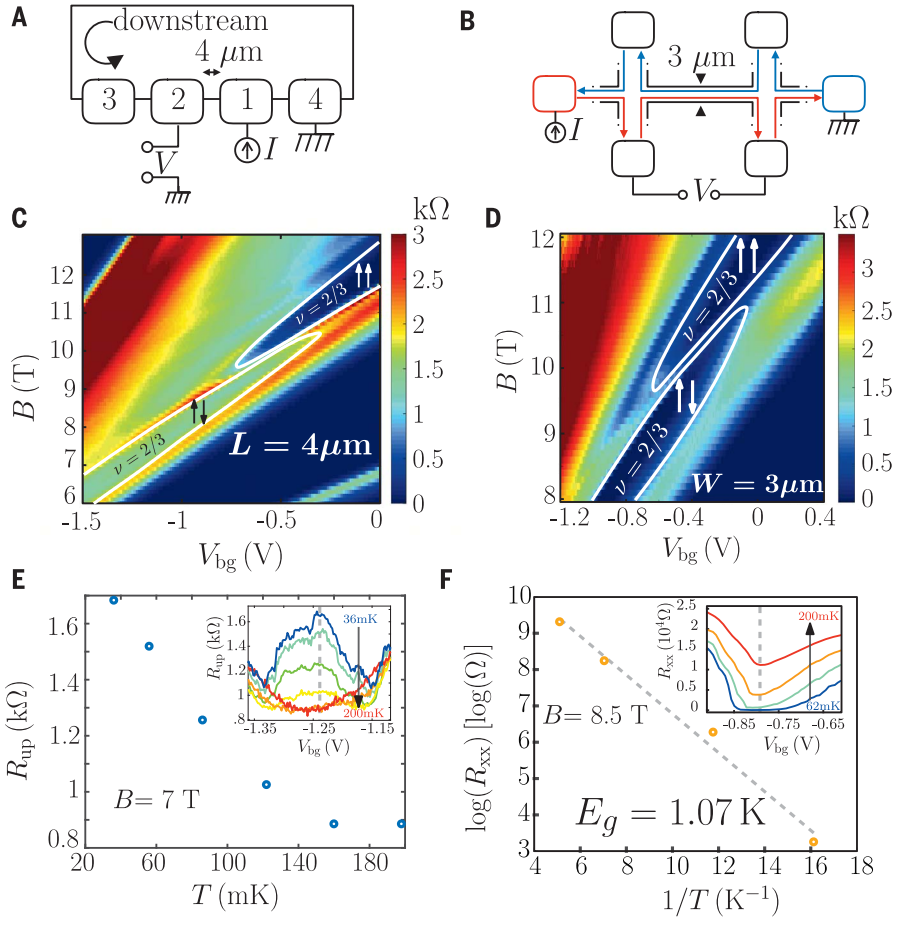

Fig. 3. Different sample geometries validating the presence of a counter-propagating charge flow. (**A**) Sketch of the three-terminal measurement. Four contacts are aligned on a single edge of the sample, 4 μm apart. Current I = 1 nA was sourced at contact 1, and voltage was measured between the contact 2 placed upstream and the ground; contact 4 was grounded, and contact 3 was floating. (**B**) Sketch of the four-terminal R_{xx} measurement on a narrow, 3-μm-wide and 25-μm-long Hall bar. The red lines represent the biased-edge channels, whereas the blue ones represent the grounded-edge channels. (**C**) Three-terminal magnetoresistance versus the backgate voltage for the measurement scheme presented in (A). A clear finite resistance appears in the unpolarized region. (**D**) Four-terminal R_{xx} versus backgate voltage for the measurement scheme presented in (B). The R_{xx} values are low in both polarized and unpolarized regions, in contrast to (C). (**E**) Evolution of the resistance measured in the unpolarized regime at B = 7 T and V_{bg} = –1.24 V as function of temperature. (Inset) Resistance in the unpolarized regime as function of the backgate voltage for different temperatures (36, 56, 86, 122, 160, and 198 mK). (**F**) Evolution of the log of the longitudinal resistance versus the inverse of the temperature in the Hall bar geometry. (Inset) Evolution of the resistance versus the backgate voltage in the unpolarized regime for several temperatures (62, 85, 142, and 196 mK). The extracted activation gap is E_g = 1.07 K.

deviation of the two-terminal resistance from the canonical value $R_{2t} \simeq 38.7$ kilohms. We therefore have conducted two-terminal resistance measurements of several samples, consisting of two 60-μm-wide ohmic contacts separated by a distance L ranging from 4 to 15 μm. The large aspect ratio (of width to length) minimizes backscattering between the propagating edge modes on opposite sides of the mesa. As visible on Fig. 2A for L = 4 μm, in the (B, V_{bg}) phase space corresponding to the polarized state, we found a two-terminal resistance $R_{2t}^{\uparrow\uparrow}(L = 4) \simeq 38.6 \pm 0.1$ kilohms. However, for the unpolarized state, the resistance plateau was found to deviate from the quantized value, showing $R_{2t}^{\uparrow\downarrow}(L = 4) \simeq 35.5$ kilohms.

Measuring the evolution of $R_{2t}^{\uparrow\uparrow}$ and $R_{2t}^{\uparrow\downarrow}$ with length, we found $R_{2t}^{\uparrow\uparrow}$ independent of contact separation (Fig. 2B, orange circles), whereas $R_{2t}^{\uparrow\downarrow}$ increases with L, approaching the quantized value for L = 15 μm (Fig. 2B, blue circles). Exponential fit of the two-terminal resistance is presented in Fig. 2B (dashed blue line), $[R(0) - R(\infty)]e^{-x/l_0} + R(\infty)$, where $R(0)$ = 20 ± 13 kilohms is the resistance at zero distance, $R(\infty)$ = 38.2 ± 0.3 kilohms is the resistance at infinite distance, and l_0 = 2.1 ± 0.8 μm is the characteristic equilibration length [additional details on Fig. 2B are provided in (*37*), section 2]. Moreover, the resistance $R(0)$ is in agreement with the two-terminal resistance predicted for unequilibrated channels proposed in (*6*), $R_{2t} = (4e^2/3h)^{-1} \approx 19.4$ kilohms. These observations might have been possible at short distance because of the reduction of scattering events and the screening of the Coulomb interaction by the back gate placed 1 μm away from the 2DEG.

Bearing in mind that a finite R_{xx} caused by dissipation processes at short contact separation can lead to similar observations, a few additional configurations were tested. One of them was a configuration that uses a complementary Hall

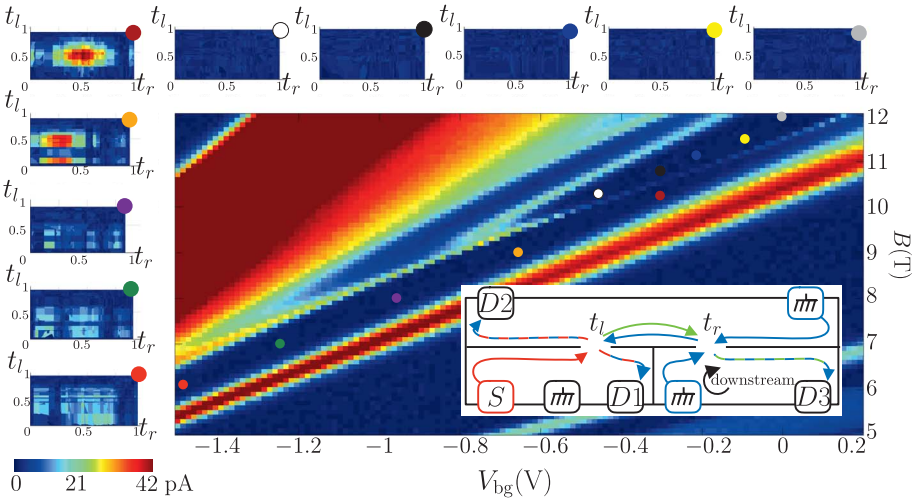

Fig. 4. Generation of upstream charge current by a quantum point contact. Evolution of the current measured in D3 as function of t_l and t_r for different points in the (V_{bg}, B) phase space (points shown in the large image). A significant current is measurable in the unpolarized region (red, green, purple, orange, and brown points), whereas no signal was measurable in the polarized region (white, black, blue, yellow, and gray points). (**Inset**) Two successive quantum point contacts setup. Current is sourced at S (red), flowing downstream to the left QPC; there, it is split to downstream (red/blue) and upstream (green) charge currents. The unequilibrated upstream current reaches the second QPC and turns back to downstream (green/blue), where we measured its voltage at D3. The sketch is not to scale; the distance between the two QPC is 700 nm, and the distance between the QPC and the nearest ohmic contact is 30 μm.

bar structure, with a narrow Hall channel width of 3 μm (Fig. 3B); this was necessary in order to ensure the lack of backscattering along distances under consideration. The measured R_{xx} (Fig. 3D) for the two $\nu = 2/3$ states by using this geometry was negligibly small, ensuring that edge states located on opposite sides of the Hall bar (Fig. 3B, red and blue lines) do not exchange particles. This observation is in agreement with the relatively large gap (~1 K for the unpolarized state) extracted from the temperature evolution of R_{xx}^{4p} presented on Fig. 3F and is in agreement with previous measurements (*38*, *39*). Furthermore, testing a Corbino geometry sample ensured a negligible bulk conductance of both $\nu = 2/3$ states [(*37*), section 3]. Last, a three-terminal configuration, with contacts aligned on a single edge of the mesa (each separated by 4 μm), allowed separation of the upstream current from the downstream one (Fig. 3A), providing a direct measurement for the upstream conductance. Current I was sourced via contact 1 and drained via contact 4 to the ground. A finite voltage V_{up} was measured at contact 2 for the unpolarized state only as visible on Fig. 3C. The resistance, defined as $R_{up} = V_{up}/I$, continuously dropped with increasing temperature up to 200 mK (Fig. 3E). This dependence has an opposite trend to that of usual dissipative processes such as variable range hopping or activation mechanisms, ruling them out as alternative explanations. A complementary measurement of the downstream resistance, $R_d = V_d/I$, was done by sourcing current via contact 2 and measuring the voltage at contact 1. The upstream and downstream conductances, calculated by using the Landauer-Buttiker formalism (*40*, *41*) [(*38*), section 4], leads to $G_d \approx 0.687\, e^2/h$ and $G_{up} \approx 0.026\, e^2/h$ or equivalent to a two-terminal resistance $(G_{up} + G_d)^{-1} \approx 1.40\ h/e^2 \approx 36.2$ kilohms, which is in agreement with the two-terminal configuration at 4 μm presented above (Fig. 2). The mobility of the 2DEG in proximity to an alloyed ohmic contact is degraded, and its density is increased, which limited us on the minimal distance between ohmic contacts to 4 μm.

In order to probe the edge modes at shorter distances, we used a configuration consisting of two, gate-defined quantum point contacts (QPCs) separated by 700 nm (Fig. 4, inset), with all ohmic contacts placed far away (above 30 μm). A current $I = 1$ nA was sourced via contact S; currents were monitored at the drains while scanning the transmissions of the left and right QPCs t_l and t_r. This was done at different points in the (V_{bg}, B) phase space for both spin polarization of the $\nu = 2/3$ states, indicated by the colored circles in Fig. 4. In the polarized state, all of the current flowed to drains D1 and D2 independent of t_r, which is consistent with downstream channels, and zero current was measured at D3 (Fig. 4, white, black, blue, yellow, and gray points). However, in the unpolarized state (Fig. 4, red, green, purple, orange, and brown points), substantial signal was found in D3, simultaneously decreasing the current measured in D1 and D2 result in overall current conservation [(*37*), section 5]. This "upstream effect" can be explained by the appearance of an upstream current between the two QPCs (Fig. 4, inset, green arrow), which emerges from the left QPC, flows a short distance to the right QPC, and scatters back to the downstream channel, finally arriving at D3. A maximum current at D3 was measured when $t_l = t_r = 0.5$ [a toy model for this effect is presented in (*37*), section 6].

The present set of experiments revealed counterpropagation of charged particles in the fractional quantum Hall effect regime. This present experiment may induce future theoretical works of the less understood unpolarized $\nu = 2/3$ state.

REFERENCES AND NOTES

1. K. V. Klitzing, G. Dorda, M. Pepper, *Phys. Rev. Lett.* **45**, 494–497 (1980).
2. D. C. Tsui, H. L. Stormer, A. C. Gossard, *Phys. Rev. Lett.* **48**, 1559–1562 (1982).
3. R. B. Laughlin, *Phys. Rev. Lett.* **50**, 1395–1398 (1983).
4. C. W. J. Beenakker, *Phys. Rev. Lett.* **64**, 216–219 (1990).
5. X. Wen, *Mod. Phys. Lett. B* **05**, 39–46 (1991).
6. A. H. MacDonald, *Phys. Rev. Lett.* **64**, 220–223 (1990).
7. R. C. Ashoori, H. L. Stormer, L. N. Pfeiffer, K. W. Baldwin, K. West, *Phys. Rev. B Condens. Matter* **45**, 3894–3897 (1992).
8. R. Sabo *et al.*, *Nat. Phys.* 10.1038/nphys4010 (2017).
9. C. L. Kane, M. P. A. Fisher, J. Polchinski, *Phys. Rev. Lett.* **72**, 4129–4132 (1994).
10. Y. Meir, *Phys. Rev. Lett.* **72**, 2624–2627 (1994).
11. J. Wang, Y. Meir, Y. Gefen, *Phys. Rev. Lett.* **111**, 246803 (2013).
12. A. Bid *et al.*, *Nature* **466**, 585–590 (2010).
13. I. Gurman, R. Sabo, M. Heiblum, V. Umansky, D. Mahalu, *Nat. Commun.* **3**, 1289 (2012).
14. H. Inoue *et al.*, *Nat. Commun.* **5**, 4067 (2014).
15. A. Rosenblatt *et al.*, *Nat. Commun.* **8**, 2251 (2017).
16. A. Grivnin *et al.*, *Phys. Rev. Lett.* **113**, 266803 (2014).
17. J. P. Eisenstein, H. L. Stormer, L. N. Pfeiffer, K. W. West, *Phys. Rev. B Condens. Matter* **41**, 7910–7913 (1990).
18. S. Kronmüller *et al.*, *Phys. Rev. Lett.* **81**, 2526–2529 (1998).
19. S. Kronmüller *et al.*, *Phys. Rev. Lett.* **82**, 4070–4073 (1999).
20. T. Chakraborty, *Adv. Phys.* **49**, 959–1014 (2000).
21. J. H. Smet, R. A. Deutschmann, W. Wegscheider, G. Abstreiter, K. von Klitzing, *Phys. Rev. Lett.* **86**, 2412–2415 (2001).
22. S. Kraus *et al.*, *Phys. Rev. Lett.* **89**, 266801 (2002).
23. J. Hayakawa, K. Muraki, G. Yusa, *Nat. Nanotechnol.* **8**, 31–35 (2013).
24. J. N. Moore, J. Hayakawa, T. Mano, T. Noda, G. Yusa, *Phys. Rev. Lett.* **118**, 076802 (2017).
25. R. S. K. Mong *et al.*, *Phys. Rev. X* **4**, 011036 (2014).
26. D. J. Clarke, J. Alicea, K. Shtengel, *Nat. Phys.* **10**, 877–882 (2014).
27. T. Wu *et al.*, *Phys. Rev. B* **97**, 245304 (2018).
28. J. K. Jain, *Phys. Rev. Lett.* **63**, 199–202 (1989).
29. I. V. Kukushkin, K. V. Klitzing, K. Eberl, *Phys. Rev. Lett.* **82**, 3665–3668 (1999).
30. B. Verdene *et al.*, *Nat. Phys.* **3**, 392–396 (2007).
31. J. Huels, J. Weis, J. Smet, K. Klitzing, Z. Wasilewski, *Phys. Rev. B* **69**, 085319 (2004).
32. S. Hennel *et al.*, *Phys. Rev. Lett.* **116**, 136804 (2016).
33. H. Cho *et al.*, *Phys. Rev. Lett.* **81**, 2522–2525 (1998).
34. Y. Q. Li, V. Umansky, K. von Klitzing, J. H. Smet, *Phys. Rev. B* **86**, 115421 (2012).
35. J. H. Smet *et al.*, *Nature* **415**, 281–286 (2002).
36. Y.-H. Wu, G. J. Sreejith, J. K. Jain, *Phys. Rev. B* **86**, 115127 (2012).
37. Supplementary text is available as supplementary materials.
38. L. W. Engel, S. W. Hwang, T. Sajoto, D. C. Tsui, M. Shayegan, *Phys. Rev. B Condens. Matter* **45**, 3418–3425 (1992).
39. G. S. Boebinger, A. M. Chang, H. L. Stormer, D. C. Tsui, *Phys. Rev. Lett.* **55**, 1606–1609 (1985).
40. M. Büttiker, *Phys. Rev. Lett.* **57**, 1761–1764 (1986).
41. S. Datta, *Electronic Transport in Mesoscopic Systems* (Cambridge Univ. Press, 1995), vol. 3.
42. A. Rosenblatt, F. Lafont, Replication Data for: Counter-propagating charge transport in the quantum Hall effect regime. Harvard Dataverse (2018);

ACKNOWLEDGMENTS

We thank A. Stern and Y. Meir for fruitful discussions. We thank D. Mahalu for her precious help in the ebeam lithography process. **Funding:** We acknowledge the European Research Council under the European Community's Seventh Framework Program,

grant agreement 339070; the partial support of the Minerva Foundation, grant 711752; and, together with V.U., the German-Israeli Foundation (GIF), grant I-1241-303.10/2014, and the Israeli Science Foundation (ISF). **Author contributions:** F.L. and A.R. contributed equally to this work in sample design, device fabrication, measurement set-up, data acquisition, data analysis and interpretation, and writing of the paper. M.H. guided the experimental work and contributed in data interpretation and writing of the paper. V.U. contributed in molecular beam epitaxy growth. **Competing interests:** The authors declare that they have no competing financial interests. **Data and materials availability:** All data needed to evaluate the conclusions in the paper are present in the paper or the supplementary materials and deposited at (*42*).

SUPPLEMENTARY MATERIALS

www.sciencemag.org/content/363/6422/54/suppl/DC1
Supplementary Text
Figs. S1 to S5

1 November 2017; accepted 8 November 2018
10.1126/science.aar3766

Counter-propagating charge transport in the quantum Hall effect regime

Fabien Lafont, Amir Rosenblatt, Moty Heiblum and Vladimir Umansky

Science **363** (6422), 54-57.
DOI: 10.1126/science.aar3766

A backward current

Two-dimensional materials in a magnetic field can exhibit the so-called quantum Hall effect. This regime is characterized by currents running along the edge of the sample in the "downstream" direction determined by the sign of the magnetic field. Lafont *et al.* studied electrical transport in GaAs-AlGaAs heterostructures, focusing on a previously less-studied spin-unpolarized state in the fractional quantum Hall regime. By considering various experimental configurations, they observed a component of the charge current flowing in the opposite, "upstream" direction.

Science, this issue p. 54